



# Fluorescence sensor for bovine serum albumin detection based on the aggregation and release of CdS QDs within CMC

Meng Cui · Yuhang Xin · Rui Song · Qiyuan Sun · Xin Wang · Dayong Lu

Received: 9 June 2019 / Accepted: 15 November 2019 / Published online: 28 November 2019  
© Springer Nature B.V. 2019

**Abstract** Here, an efficient in vitro fluorescence biosensor for bovine serum albumin (BSA) based on the aggregation and release of CdS quantum dots (QDs) within carboxymethyl cellulose (CMC) was investigated and discussed. The aggregation of CdS QDs within CMC was prepared by electrostatic interaction. The release of CdS QDs was due to strong covalent linking between BSA and CMC, thus leading to the more favorable combination of BSA and CMC in the system with the presence of BSA. The detection of BSA was based on the quenching and recovery of fluorescence intensity in the system, which was caused by the aggregation and release of CdS QDs. An excellent linear relationship ( $R^2 = 0.99286$ ) was obtained between fluorescence intensity and BSA concentration (0.05–2.00  $\mu\text{M}$ ) with a detection limit of  $10^{-8}$  M. In addition, the detection method showed high selectivity towards BSA and good stability. These results suggest that the method can be utilized as an efficient and highly selective reagent for quantification of BSA for in vitro biological science.

**Keywords** Composite microspheres · Fluorescent sensor · Carboxymethyl cellulose (CMC) · Quantification of BSA · Electrostatic interaction

## Introduction

Protein which plays a vital role in biological activities is an important constituent of cells. Of all the proteins, serum albumin is the most abundant in mammal blood (Carter and Ho 1994; Nicholson and Wolmarans 2000; Gu et al. 2017). It acts as a depot and is used as transport for a large number of endogenous and exogenous compounds in the circulation system. Therefore, the quantification analysis for serum albumin is crucial. BSA is composed of 582 amino acid residues with 17 cysteine cross-linked residues and 1 free cysteine, and its secondary structure is the most analogous to human serum albumin (HSA). It has an important role in maintaining osmotic pressure balance and buffered pH (Guo and Shen 1999; Li et al. 2006; Liu et al. 2006). Owing to the numerous applications of BSA, its determination has been well studied.

Until now, many methods for the detection of BSA in vitro have been proven. Zhu reported a simple label-free fluorescent biosensor based on Au nanorods (Au NRs) for the assay of BSA. In that study, the Au NRs coated by mesoporous silica were loaded with acridine orange and the detection of BSA was based on the

---

M. Cui · Y. Xin · R. Song · Q. Sun · X. Wang · D. Lu (✉)

Research Center of Material Sciences and Engineering,  
Jilin Institute of Chemical Technology, Jilin 132022,  
People's Republic of China  
e-mail: 421117044@qq.com

quenching of the fluorescence signal. The results showed that the values of the fluorescence intensity from the biosensor were proportional to various concentrations of BSA, and the limit of detection (LOD) was 0.25 M (Zhu et al. 2015a). Sasmal demonstrated an electrical detection method for ultra-low BSA based on solution-processed zinc oxide nanospheres. The device worked with different concentrations of BSA based on the variation in the conductivity of the ZnO nanospheres and displayed a good sensitivity, with a LOD of 10 pM (Sasmal et al. 2015). Ni reported a BSA detection method with GO-based 10-hydroxy camptothecin (HCPT). They proposed that in the presence of graphene oxide (GO), the delivery of HCPT to BSA was improved. Thus, a biosensing platform for BSA fluorescence detection was constructed (Ni et al. 2013). Among the various detection methods, fluorescence biosensors are the simplest and have numerous advantages, such as high selectivity and good sensitivity. Thus, developing appropriate fluorescence biosensors for BSA and other proteins has attracted increased attention (Yan et al. 2017; Achadu and Nyokong 2017; Liu et al. 2017a; Zhang et al. 2017a). Until now, carbon dots (Yang et al. 2015; Liu et al. 2015a), gold nanoclusters (Liu et al. 2015b; Selvaprakash and Chen 2014), rare earth elements (Weng and Yan 2016; Refat et al. 2014; Liu et al. 2016a) and graphene quantum dots (QDs) (Liu et al. 2016b; Chen et al. 2016) have been considered as prospective fluorescence donors for fabricating fluorescence biosensors. Among the fluorescent materials mentioned above, water-soluble semiconductor QDs are promising candidates for biosensing, owing to their excellent characteristics including large surface area, low cost, water solubility, chemical inertness and excellent photo-stability (Lu et al. 2017; Zhang et al. 2017b; Ratnesh and Mehata 2017). At present, these materials have been widely explored as luminophores for fluorescence biosensors (Wang et al. 2017; Mehrzad-Samarin et al. 2017; Liu et al. 2017b; Ngamdee et al. 2017; Yang et al. 2017). However, there are still some challenges to using QDs for biological studies. Among them the most prominent are: developing hydrophilic QDs that are luminescent with surface chemistry adaptable to varied biological applications, designing versatile techniques for biomolecules, and demonstrating that QDs do not interfere with normal physiology. Therefore, modifying QDs to increase their biocompatibility and reduce

their toxicity has become a problem that must be solved quickly. Studies have indicated that after coating with biocompatible polymer, the toxicity of the QDs is effectively inhibited, and the modified QDs can be utilized in biological sciences (Jaiseal et al. 2003; Wang et al. 2002; Gao and Nie 2004; Adegoke et al. 2017). Many reports about QD bioconjugates that can be used for numerous *in vitro* assays were proposed (Gao et al. 2004; Yu et al. 2007) and the choice of the polymer for modifying the QDs is critical.

Cellulose and its derivatives are widely used in the biomedical field. They are promising hosts for modification with QDs for fabricating biosensors, owing to their excellent non-toxicity and good biocompatibility (Jasim et al. 2017; Chee 2016; Cui et al. 2011). The most commonly used cellulose derivatives are cellulose ethers, particularly CMC, which can be easily dissolved in water and is negatively charged due to the presence of  $-\text{COO}^-$ . Thereby, CMC exhibits environmental friendliness, is non-allergenic and non-toxic, has good biocompatibility. This means it can be used for a wide range of applications, such as drug delivery, skin care products, papermaking, food additives, and drug formulations (Nie et al. 2004; Biswal and Singh 2004). More importantly, CMC contains abundant functional groups, and can combine with charged materials utilizing anionic–cationic electrostatic attraction. CMC can also be covalently bonded to appropriate macromolecules to obtain CMC-based composite materials. Preparing a CMC/QDs composite by coating CMC on QDs can effectively inhibit toxicity and the obtained CMC/QDs maintain the advantages of CMC and QDs, such as strong stability and high strength (Li et al. 2016; Phukn et al. 2014; Yadav et al. 2013; Coleman et al. 2006; Han et al. 2011a, b; Zhu et al. 2015b). In addition, the transformation of fluorescence intensity caused by the composite is easy to detect, which provides a convenient signal for the fabrication of biosensors.

In recent years, many researchers have been devoted to studying polymer-semiconductor QD composites. The composite synthesis methods used in a majority of the studies are through the linkage of functional groups (Mansur et al. 2017) and coordination reactions (Li et al. 2015). However, for the methods above, the reaction processes are quite difficult to control, and the reaction conditions are complicated. Moreover, the inflexibility of the

composite limits the applications. For the process of linking functional groups, the chief work needed is the modification of the QDs. However, appropriate chemical reaction conditions of the modification processes need to be strictly controlled. In addition, the conditions for the linking between functional groups of the modified QDs and polymers are even harsher and include higher temperatures, acidic or alkaline environments (Jia et al. 2017) and inert atmospheres (Guo et al. 2017). For the coordination reaction, the uniform dispersion of QDs in polymer is hard to achieve (Tang et al. 2016). Therefore, an easily controlled and uncomplicated method is greatly favored by researchers. LbL self-assembly is a simple and controllable method. Self-assembly is driven by various factors such as the electrostatic attraction between anion and cation, hydrogen bonding, or bond cooperation. Therefore, in this work, the fabrication of CMC and QDs was carried out by LbL self-assembly.

In this paper, water-soluble CdS QDs with surface enrichment of positive charges are synthesized successfully, and the core-shell fluorescence composite microspheres of CdS QDs and CMC are obtained via the driving force of electrostatic attraction between anion and cation. In order to ensure complete assembly between CdS QDs and CMC, the structure and properties of the products obtained are characterized by FT-IR, XRD, FS, DTG and DSC. Then, the composite microspheres are successfully used for the accurate detection of BSA *in vitro*. Particularly, selectivity experiments involving several interfering drugs were carried out, and the results showed that the core-shell composite fluorescence biosensor displays high selectivity towards BSA. Also, the results from the stability experiment show the CdS/CMC composite microspheres exhibit a low fluorescence quenching after standing for 1 month. Also, two standard BSA reagents for clinical are detected with the method we developed. The detected concentration is highly consistent with the standard concentration. Therefore, these results suggest that the method can be utilized as an efficient and highly selective reagent for quantification of BSA *in vitro*.

## Experimental section

### Materials

Cadmium chloride ( $\text{CdCl}_2$ ) and sodium sulfide ( $\text{Na}_2\text{S}$ ) were purchased from the DAMAO Chemical Reagent Co. (Tianjin, China). Trisodium citrate dihydrate ( $\text{Na}_3\text{C}_6\text{H}_5\text{O}_7 \cdot 2\text{H}_2\text{O}$ ) was purchased from the YONGDA Chemical Reagent Co., Ltd. (Tianjin, China). Sodium hexametaphosphate ( $(\text{NaPO}_3)_6$ ) was purchased from the RUIJINTE Co., Ltd. (Tianjin, China). BSA standard reagent (5 mg/mL) was bought from Solarbio. BSA standard reagent (10 mg/mL) was bought from RuJi Biological Technology Co., Ltd. (Shanghai, China). All of these reagents were analytical grade and were used as received, without further purification.

The ZnS was synthesized with  $\text{C}_4\text{H}_6\text{O}_4\text{Zn}$  via a hydro-thermal method.  $\text{MoS}_2$  was synthesized with  $\text{MoCl}_5$  via an oil dissolving method. PbS was prepared by solution synthesis using PbO.  $\text{C}_4\text{H}_6\text{O}_4\text{Zn}$ ,  $\text{MoCl}_5$  and PbO which were purchased from DAMAO Chemical Reagent Co. (Tianjin, China).

The CMC used in this study was prepared with a slurry process in a solution of isopropyl alcohol with the subsequent processes of alkalization, etherification, neutralization, and washing of cellulose in our laboratory.

### Instruments

Transmission electron microscopy (TEM) images of CdS QDs and CdS/CMC microspheres were obtained using a JEM 1200EX transmission electron microscope manufactured by Japanese Electronics Co., Ltd. A Cary Eclipse fluorospectrophotometer, bought from VARIAN Co. (Santa Clara, USA) was used to measure the fluorescence intensity. Zetasizer Nano S, bought from Malvern Co. (Malvern, UK) was used to measure the zeta potential. X-ray diffraction (XRD) measurements were performed using a DX2000 X-ray diffractometer (Haoyuan, Dandong, China). The thermal properties were studied using a METTLER TGA/DSC 1 SF/1382 thermogravimetric analyzer (Mettler Toledo Co. Switzerland).

### Preparation of CdS quantum dots

CdS QDs were synthesized in a one-step facile process. Namely, certain amounts of  $\text{CdCl}_2$ ,

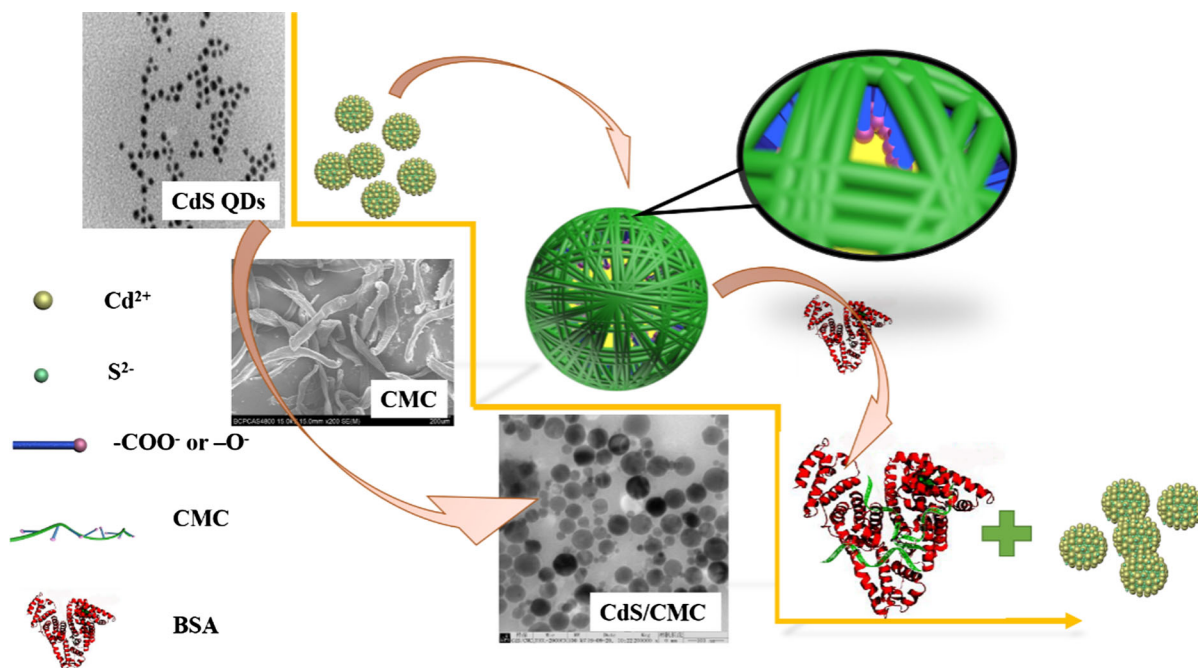
$\text{Na}_3\text{C}_6\text{H}_5\text{O}_7 \cdot 2\text{H}_2\text{O}$ ,  $(\text{NaPO}_3)_6$  and  $\text{NaS}$  were thoroughly dissolved in distilled water under vigorous stirring to obtain homogeneous solutions. After that, the solutions of  $\text{CdCl}_2$ ,  $\text{Na}_3\text{C}_6\text{H}_5\text{O}_7 \cdot 2\text{H}_2\text{O}$ , and  $(\text{NaPO}_3)_6$  were mixed in a beaker by vigorous stirring for 5 min in an ice water bath at 4 °C. The solution of  $\text{NaS}$  was then added slowly into the mixed solutions while stirring at room temperature for 30 min to obtain  $\text{CdS}$  QDs. Finally, the obtained  $\text{CdS}$  QDs were preserved at room temperature for further characterization and use.

### Synthesis of $\text{CdS}/\text{CMC}$ microspheres

The CMC solution was prepared by dispersing 1 g of CMC in distilled water, while stirring at 90 °C. To obtain  $\text{CdS}/\text{CMC}$  composite microspheres, the stock solutions of  $\text{CdS}$  QDs and CMC were mixed at a certain mass ratio, at room temperature. The obtained  $\text{CdS}/\text{CMC}$  composite microspheres were preserved until further characterization and use. The composite mechanism and the appearance of the samples obtained are shown in Scheme 1.

### Application of the FBSs for BSA bioanalysis

Fabrication of the studied FBSs is shown in Scheme 1. After being dissolved in aqueous solution, CMC exhibits negative charge. It was coated on the surfaces of  $\text{CdS}$  QDs with  $\text{Cd}^{2+}$  enrichment by the electrostatic attraction of anions and cations, forming the  $\text{CdS}/\text{CMC}$  core-shell composite system. Due to the coating effect of CMC, the fluorescence properties of  $\text{CdS}/\text{CMC}$  composites are greatly attenuated compared with that of free  $\text{CdS}$  QDs. BSA has a typical heart-shaped structure with many sites that can bind with CMC. It is composed of two parts, with a 1 nm wide slit exits between them. Among the sites in BSA, Trp-213 and Trp-134 have the most significant binding effect with CMC. Trp-213 is primarily located in the slit cavity with positive charge, and it is the main binding site of the anions. So, when  $\text{CdS}/\text{CMC}$  composites are added to the system, CMC surrounds the Trp-213 and gradually forms aggregates which are absorbed into the slits and inner cavities of BSA. This aggregation is stronger than the electrostatic attraction of anions and cations, so CMC is more inclined to combine with BSA, and the  $\text{CdS}$  QDs are released back into the system. With the release of  $\text{CdS}$  QDs, the fluorescence intensity of the system is restored, and the



**Scheme 1** The mechanism of  $\text{CdS}/\text{CMC}$  FBSs for BSA sensing

recovery of fluorescence intensity corresponds to the content of BSA added in the system. This can be used to detect BSA by detecting the fluorescence intensity of the system.

### The sensing process

Freshly prepared mixture containing 1 g/mL CdS/CMC composite microspheres was used for BSA detection. In this mixture, BSA was added at different concentrations (range, 0.05–2.00  $\mu\text{M}$ ). The mixture was stabilized for 30 min at room temperature before taking spectral measurements. The fluorescence intensity was measured at  $\lambda_{\text{em}}/\lambda_{\text{ex}} = (350 \text{ nm})/(470 \text{ nm})$ . The selectivity of the synthesized FBSs towards BSA was also examined. Vitamin B<sub>6</sub>, coumarin, tetracycline, melamine, ZnS, MoS<sub>2</sub>, PbS, Cu<sup>2+</sup>, Fe<sup>3+</sup> and Al<sup>3+</sup> (concentration tenfold of BSA) were added to the solution, and their fluorescence intensity was measured. Each experiment was repeated three times.

## Results and discussion

### Characterization of CdS QDs with surface enrichment of Cd<sup>2+</sup>

XRD was used to quantify the lattice structure of the prepared CdS QDs, and the obtained spectrum is shown in Fig. 1a. The XRD spectrum of CdS QDs exhibits three sharp diffraction peaks, at 26.7°, 44.1°, and 51.7°, which correspond to the typical crystal

planes of CdS QDs: (111), (220), and (311), respectively (Junaid et al. 2019). The slight diffusion of these diffraction peaks was consistent with the small size of CdS QDs, which, in turn, was consistent with the following TEM results. The crystal structure and the small size of the synthesized CdS QDs yield higher stability of CdS QDs-based nanocrystals in composite materials.

One of the unique optical properties of semiconductor QDs is that the spectral peak positions of the QDs are tunable. Unlike macroscale structures, their emission spectra positions depend on their size and material composition (Robelek et al. 2004; Ding et al. 2003; Yu et al. 2006). Once the QDs change size, their emission spectra positions shift distinctly. Figure 1b shows the fluorescence spectra (FS) of CdS QDs, with the excitation wavelength ranging from 360 to 450 nm. In Fig. 1b, the maximal emission peak shifts from 525 to 575 nm as the excitation wavelength is changed. The shift is less than the 70 nm shift for other semiconductor QDs, which confirmed that the synthesized CdS QDs are relatively homogeneous. In addition, the quantum yield (QY) of CdS QDs was measured according to an established procedure (Dong et al. 2015). Rhodamine B in ethanol (literature quantum yield is 95% at 480 nm) is chosen as the standard. Absolute values of QY are calculated with the reference Rhodamine B solution, which has a fixed and known fluorescence QY value, according to the equation below:

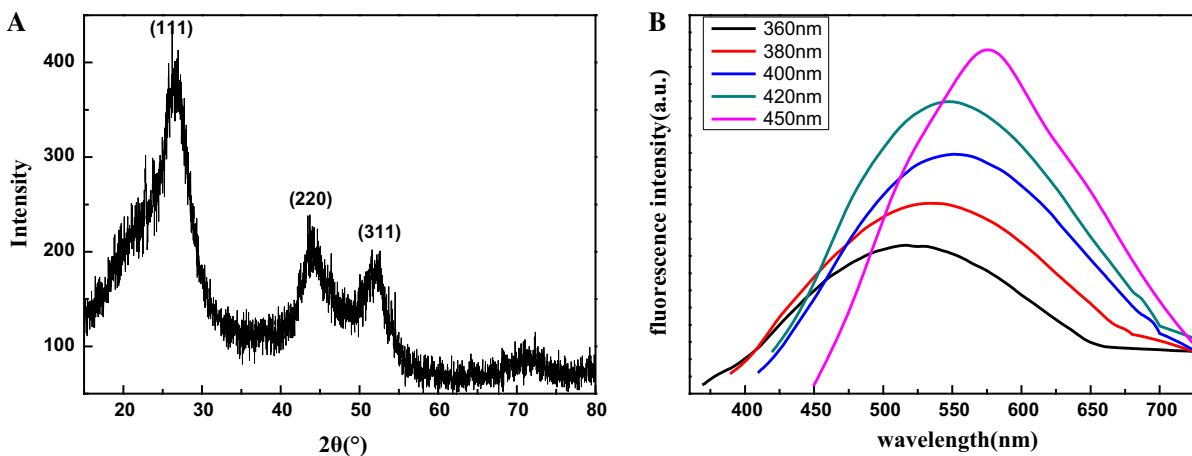


**Fig. 1** a The XRD spectrum, and b the fluorescence intensity of the synthesized CdS QDs



$$Y_u = Y_s \times \left(\frac{F_u}{F_s}\right) \times \left(\frac{A_s}{A_u}\right) \times \left(\frac{G_u}{G_s}\right)$$

Where  $Y_u$  is the QY of CdS QDs,  $Y_s$  is the QY of Rhodamine B,  $F_u$  and  $F_s$  are the integral areas of the fluorescence emission spectrum of CdS QDs and Rhodamine B,  $A_u$  and  $A_s$  are the values of absorbance at this excitation wavelength of CdS QDs and Rhodamine B,  $G_u$  and  $G_s$  are the values of the refractive index of the solvent of CdS QDs and Rhodamine B. The obtained QY of CdS QDs was 27%. The reported QY of water-soluble CdS QDs was 20–30% (Mao et al. 2008; Wang et al. 2011). Thus, the CdS QDs obtained by the experiment above has a relatively high QY.

### Characterization of CdS/CMC microspheres

#### XRD patterns of CdS/CMC microspheres

The XRD patterns of the pure CMC, CdS QDs and CdS/CMC microspheres are presented in Fig. 2. The XRD patterns are collected from  $3^\circ$  to  $70^\circ$  ( $2\theta$ ). The curves of the pure CMC do not show any clear sharp peaks in the XRD patterns, which reflected the amorphous structure of the CMC. In the curve of the CdS/CMC composite microspheres, the patterns are quite similar to the pure CMC. It is also obvious that clear sharp peaks at  $24.5^\circ$ ,  $30.7^\circ$  and  $43.9^\circ$  appear in the curve of the CdS/CMC composite microspheres. Compared with CdS QDs, the peaks are slightly shifted, which indicates that the CdS QDs are loaded

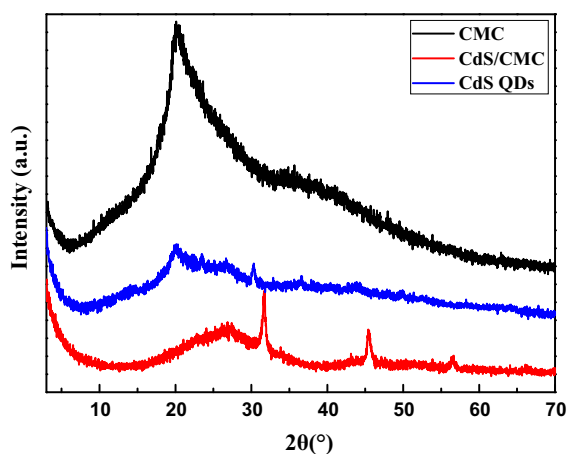


**Fig. 2** The XRD patterns of pure CMC, CdS QDs and CdS/CMC composite microspheres

into the CMC matrix, and the CdS/CMC composite microspheres were formed, so the structural regularity is enhanced.

#### FT-IR spectra of the pure CMC and CdS/CMC microspheres

The most significant transmittance bands of the infrared spectra for the three types of materials are identified through comparisons of the FT-IR data, which can be seen from Fig. 3. In Fig. 3a, a broad absorption peak at  $3450\text{ cm}^{-1}$  occurs, and the peak is due to the stretching frequency of the O–H group. The peaks at  $2928$  and  $1707\text{ cm}^{-1}$  are due to C–H and  $\text{COO}^-$  groups, respectively. The peaks at  $1420$  and  $1309\text{ cm}^{-1}$  are assigned to the  $\text{CH}_2$  scissoring and O–H bending vibrations, respectively. The band at  $1063\text{ cm}^{-1}$  is attributed to  $\text{CH}_2\text{OCH}_2$  stretching. As shown in Fig. 3c, the peaks at  $3423$  and  $1479\text{ cm}^{-1}$  could be attributed to O–H and P=O in sodium citrate and trisodium citrate dihydrate which are crude materials in the process of synthesizing of CdS QDs, respectively. The significant peak at  $943\text{ cm}^{-1}$  in the fingerprint region might be attributed to the Cd-S band. The spectrum in Fig. 3a represents the FT-IR spectrum of the pure CMC. In the spectra of b, it could be clearly observed that all the bands in CdS QDs and CMC are presented in the CdS/CMC composite microspheres. Therefore this proved that CdS QDs and CMC are completely represented in the CdS/CMC composite microspheres.

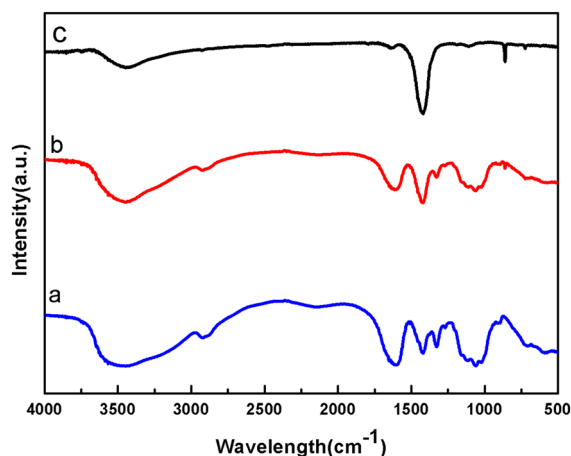


**Fig. 3** The FT-IR of CdS QDs, the pure CMC and CdS/CMC composite microspheres

### Morphology and surface potential analysis

TEM was performed to characterize the micromorphology of CdS QDs and CdS/CMC composite microspheres and to determine their size and shape distribution. The results are shown in Fig. 4. It is obvious in Fig. 4a that the CdS QDs are uniformly dispersed in solution, and the diameter of the CdS QDs are distributed in a narrow range of 3–5 nm, with the average diameter of 3.8 nm. The TEM image inset in Fig. 4a gives evidence for the single-crystalline structure of CdS QDs. A crystal plane spacing of 0.18 nm fits well with the CdS (111) facet. The TEM image of CdS QDs shows the network of CdS. According to Fig. 4b, CdS/CMC composite microspheres are relatively spherical with a monodispersed particle size distribution. It could be seen obviously from Fig. 4 that the CdS/CMC composite microspheres have a bigger size than CdS QDs. This means that in the structure of the composite microspheres, the CMC coating is on the surface of the CdS QDs. Therefore, the TEM images suggest that CMC evenly covers the CdS QDs.

### Dynamic light scattering (DLS) and zeta potential analyses

The dispersion time of colloidal particles with different sizes is different in solution. The intensity of scattered light from the laser that penetrates the solution containing the particles is detected by DLS with a time function to measure the hydrodynamic particle size distribution. The intensity of the light being scattered depends on the dispersion time, and DLS provides a correlation function that corresponds

to the particle size. The technique can be used to measure the particle size distribution. The hydrodynamic particle size distribution cylindrical graphs for CdS QDs, CMC polymer, and CdS QDs/CMC composite microspheres are shown in Fig. 5a–c. Figure 5 shows that each cylindrical graph presents a relatively narrow hydrodynamic size distribution, and the results obtained are  $3.4 \pm 0.9$  nm for CdS QDs,  $1016 \pm 495$  nm for CMC and  $25.1 \pm 1.6$  nm for CdS QDs/CMC composite microspheres. The values obtained by DLS are quite close to the results obtained by TEM. Because of this, it is concluded that the CdS QDs and CdS/CMC composites are monodispersed and non-agglomerated.

The values of zeta potential for the particles above were also measured to evaluate the colloidal stability of the nanoparticles, and the results are shown in Fig. 5a1–c1. The general guidelines that were used for zeta potential are as follows: highly stable =  $\pm 30$  mV, moderately stable = 20–30 mV, relatively stable = 10–20 mV, highly unstable = 0–10 mV. The values shown in Fig. 5a1–c1 are:  $31.2 \pm 4.6$  mV for CdS QDs,  $-92.4 \pm 12.1$  mV for CMC,  $-56.9 \pm 7.8$  mV for CdS/CMC composite microspheres. The zeta potential values show that the particles are relatively within the high colloidal stability. The zeta potential also suggests that CdS QDs are indeed coated with CMC.

### Thermogravimetric analysis

DTG and DSC are taken to investigate the thermogravimetric properties of CMC and the CdS/CMC composite microspheres, and the results are presented in Fig. 6. According to Fig. 6a, the DTG curves of

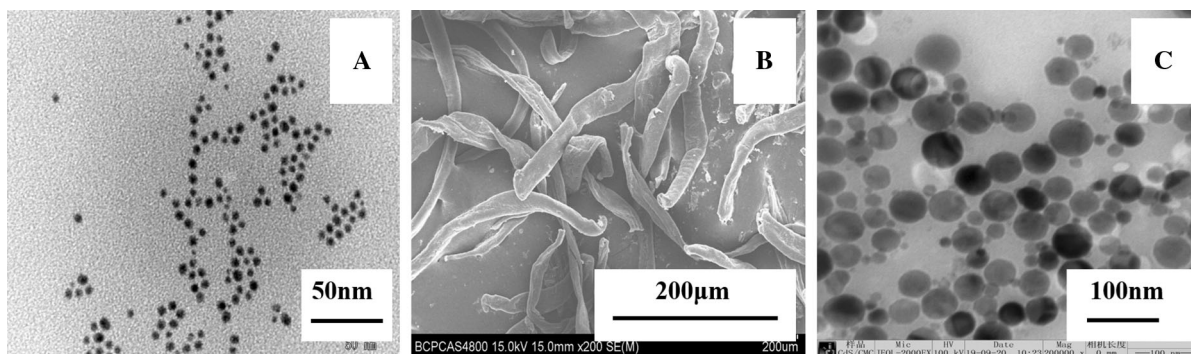


**Fig. 4** Morphology of **a** CdS QDs, **b** CMC, and **c** CdS/CMC microspheres

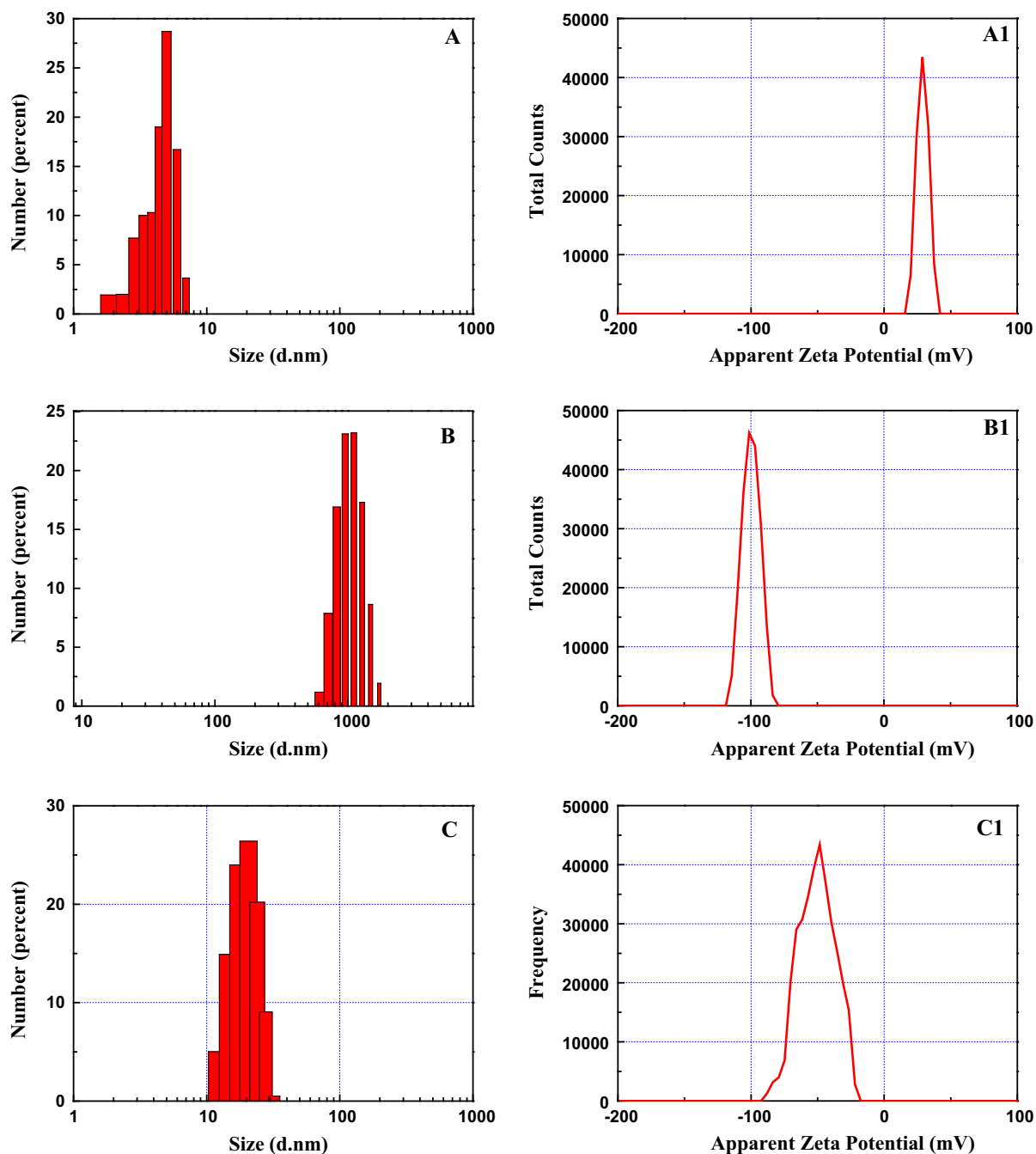


**Fig. 5** DLS and zeta potential of CdS QDs, the pure CMC and CdS/CMC composite microspheres

CMC and the CdS/CMC composite microspheres all exhibit three peaks which indicate that the degradation of CMC and CdS/CMC composite microspheres occurred in three steps. The first peak of weight loss at about 100 °C might have been due to loss of absorbed water. Then, the weight loss rate increased

with increasing temperature from 210 to 310 °C. From the curve of the pure CMC, the decomposition temperature was found to be 245 °C, which is significantly lower than the decomposition temperature of the CdS/CMC composite microspheres. In addition, it is clear that the thermal decomposition rate



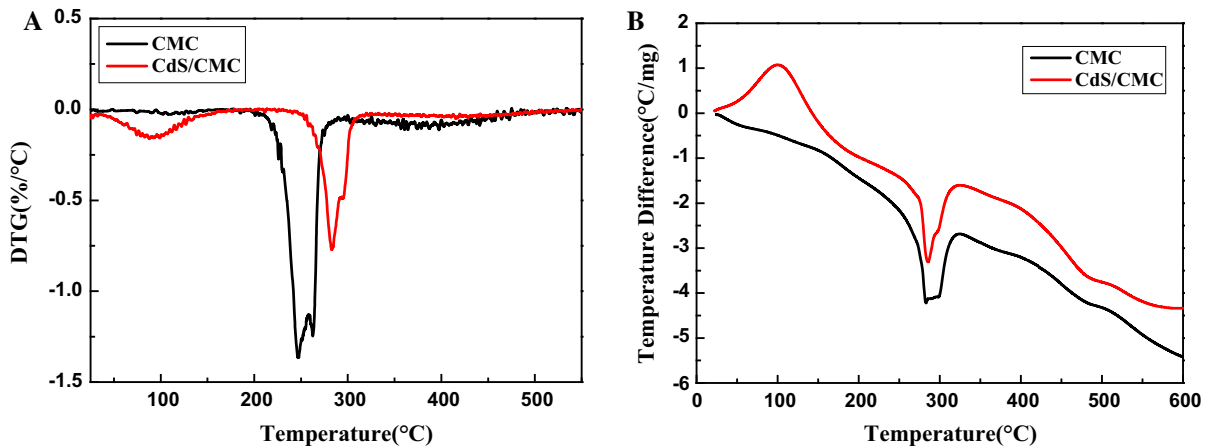


**Fig. 6** a DTG and b DSC of the pure CMC and CdS/CMC composite microspheres

of weight loss is higher than the CdS/CMC composite microspheres which indicates that when CdS QDs are added in the CMC structure, the thermal stability of the composite system is higher. In Fig. 7b, the DSC results are presented. From Fig. 7b, the curve of CdS/CMC composite microspheres exhibits two obvious peaks including an endothermic peak and an exothermic peak. When CMC is coated on the surface of the CdS QDs, a relatively ordered structure of microspheres is formed, and with the increasing temperature the microcrystalline structure was transformed. Based on this, the first peak occurred. For CMC, the structure is relatively disordered and there were no peaks indicating a structural change occurred. The second peak is from thermal decomposition, and there is not much difference between the seven samples. From the

above analysis, it is shown that CdS/CMC composite microspheres obtained were stable in a wide temperature range and can potentially be applied to wider temperature conditions.

Based on the results from FT-IR, XRD, FS, DTG and DSC it was concluded that the CdS/CMC composite microspheres that were obtained have well dispersed, uniformly spherical, and relatively stable properties and an obvious fluorescence quenching. Afterwards, the CdS/CMC composite microspheres were used to fabricate the FBS for the detection of BSA below.

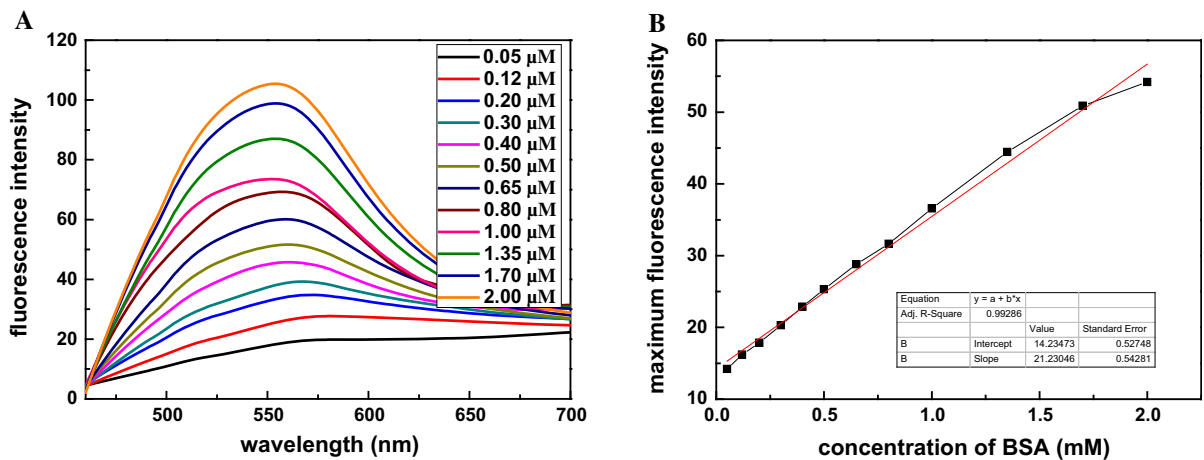


**Fig. 7** The fluorescence intensity of the proposed FBSs, for different concentrations of BSA (a) and the linear condition (b)

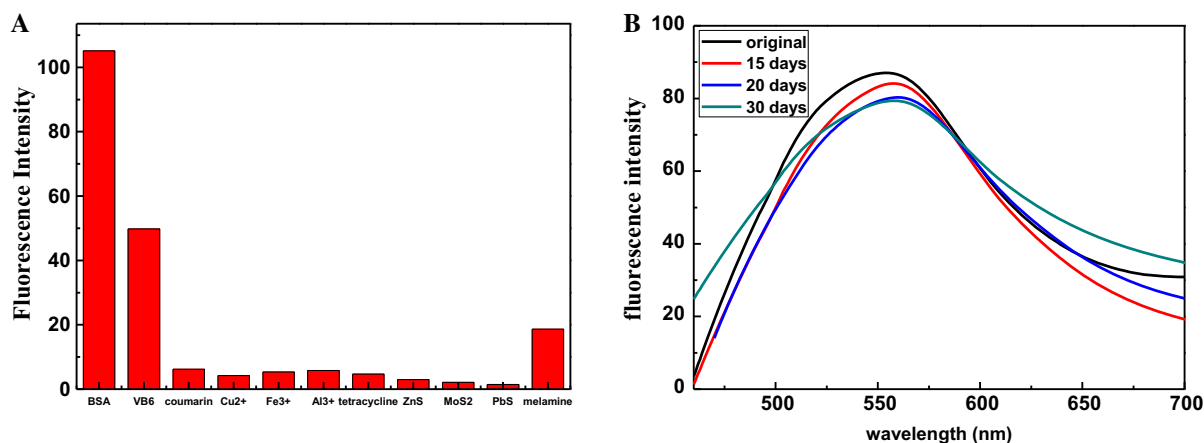


**Fig. 8** **a** Selectivity and **b** stability of the proposed CdS/CMC fluorescence biosensor

Using the synthesized CdS/CMC FBSs for BSA sensing

To explore the potential applications of the CdS/CMC FBS for BSA, the fluorescence intensities were measured for different concentrations of added BSA, and the results are shown in Fig. 7a. As shown in Fig. 7a, the fluorescence intensity of the system increased linearly with the increasing concentration of BSA. The linear range for determining BSA was 0.05–2.00  $\mu\text{M}$ . The linear equation was  $FL = 21.23046 C_{\text{BSA}} + 14.23473$ , with a statistically significant correlation coefficient of 0.99286. The limit of detection is as low as  $10^{-8}$  M, as shown in Fig. 8b. The limit of detection is calculated as  $\text{LOD} = (3\sigma/s)$ . In this equation,  $s$  corresponds to the slope of the standard curve, and  $\sigma$  corresponds to the standard deviation of the blank signal. Over four experiments, the standard deviation was 3.75%, which confirms that the proposed FBS towards BSA exhibited excellent accuracy and repeatability.

Selectivity and stability of the synthesized FBSs

The selectivity of the synthesized FBSs was also examined, and the results are shown in Fig. 8a. The fluorescence intensities of the systems with the presence of vitamin B<sub>6</sub>, coumarin, tetracycline, ZnS, MoS<sub>2</sub>, PbS, Cu<sup>2+</sup>, Fe<sup>3+</sup>, Al<sup>3+</sup> and melamine (concentration tenfold of BSA) are much weaker than that of the system with BSA. As shown in Fig. 8a, neither of the interfering substances affect the fluorescence intensity of the system. Based on this, it was concluded that the synthesized CdS/CMC FBSs display a high selectivity for BSA. This suggested that the proposed method can be used for designing BSA sensors.

To determine the stability of the proposed FBS, FS was used (Fig. 8b). There was no observed change in the peak intensity associated with BSA. After 7 days, the intensity decreased by  $\sim 2.2\%$  relative to the initial intensity. After 15 days, the intensity decreased by  $\sim 3.87\%$ , and the intensity decreased by  $\sim 6.49\%$  after 20 days. The FBS retains about 92% of its original activity after 30 days, which indicated that the proposed CdS/CMC FBS was highly stable.

**Table 1** Comparison between the concentration detected by CdS/CMC fluorescent biosensor and the concentration of standard reagent

	Standard concentration (mg/mL)	Detection concentration (mg/mL)	Deviation (%)
Reagent 1	5	4.976	0.48
Reagent 2	10	9.843	1.57

## Detection of practical standard reagents

In order to prove the accuracy and feasibility of the BSA detection method in vitro, the contents of BSA in two practical BSA standard reagents are detected. The detection result is given in Table 1. It can be seen from Table 1 that, for two standard reagents widely used in biological medicine, the deviation between BSA concentration and standard concentration obtained by our method is less than 2%. These results reasonably demonstrated that the fluorescent biosensor and the detection method that was proposed can be used for in vitro detection of BSA effectively.

## Conclusions

In conclusion, a fluorescence biosensor based on CMC-coated CdS QD composite microspheres has been successfully prepared using a LbL self-assembly process for the first time. The determination of BSA is based on the quenching and recovery of fluorescence intensity in a system which uses the competition between CdS QDs and BSA to form a composite with CMC. The results from the fluorescence intensity of systems with different concentrations of BSA suggested that the obtained CdS/CMC composite microspheres were an effective biosensor for BSA. A linear relation between the fluorescence intensity and BSA concentration is 0.05–2.00  $\mu\text{M}$  with a detection limit of  $10^{-8}$  M. In addition, the composite microspheres showed high stability with a low fluorescence quenching of 7.79% for 1 month. These results suggest that CdS/CMC composite microspheres can be utilized as efficient fluorescence biosensors for detection of BSA. The method reported in this paper is simple and efficient, which makes it an effective method for other biomolecule detection.

**Acknowledgments** This work is supported by the Changbai Mountain Scholars' Special Fund (No. 2015047).

## References

Achadu OJ, Nyokong T (2017) Graphene quantum dots coordinated to mercaptopyrindine-substituted phthalocyanines: characterization and application as fluorescence “turn ON” nanoprobe. *Spectrochim Acta Part A* 174:339–347

- Adegoke O, Morita M, Kato T et al (2017) Localized surface plasmon resonance-mediated fluorescence signals in plasmonic nanoparticle-quantum dot hybrids for ultrasensitive Zika virus RNA detection via hairpin hybridization assays. *Biosens Bioelectron* 94:513–522
- Biswal DR, Singh RP (2004) Characterisation of carboxymethyl cellulose and polyacrylamide graft copolymer. *Carbohydr Polym* 57:379–387
- Carter DC, Ho JX (1994) Structure of serum albumin. *Adv Protein Chem* 45: 153–176, 176a, 176b, 176c, 176d, 176e, 176f, 176g, 176h, 176i, 176j, 176k, 176l, 177–203
- Chee GJ (2016) A novel whole-cell biosensor for the determination of trichloroethylene. *Sens Actuators B* 23:836–840
- Chen SF, Chen XQ, Xia TT et al (2016) A novel electrochemiluminescence sensor for the detection of nitroaniline based on the nitrogen-doped graphene quantum dots. *Biosens Bioelectron* 85:903–908
- Coleman JN, Khan U, Blau WJ et al (2006) Small but strong: a review of the mechanical properties of carbon nanotube-polymer composites. *Carbon* 44:1624–1652
- Cui M, Wang FJ, Shao ZQ et al (2011) Influence of DS of CMC on morphology and performance of magnetic microcapsules. *Cellulose* 18:1265–1271
- Ding SY, Jones M, Tucder MP et al (2003) Quantum dot molecules assembled with genetically engineered proteins. *Nano Lett* 3:1581–1585
- Dong YG, Yang JL, Ding YL et al (2015) Size-controllable synthesis of highly fluorescent carbon quantum dots in a reverse microemulsion. *Chin J Lumin* 36:157–162
- Gao XH, Nie SM (2004) Quantum dot-encoded mesoporous beads with high brightness and uniformity: rapid readout using flow cytometry. *Anal Chem* 76:2406–2410
- Gao XH, Cui YY, Levenson RM et al (2004) In vivo cancer targeting and imaging with semiconductor quantum dots. *Nat Biotechnol* 22:969–976
- Gu XM, Chen Q, Fang ZJ (2017) A novel fluorescent probe based on  $\beta$ -C-glycoside for quantification of bovine serum albumin. *Dyes Pigments* 139:334–343
- Guo ZX, Shen HX (1999) A highly sensitive assay for protein using resonance light-scattering technique with dibromohydroxyphenylfluorone–molybdenum(VI) complex. *Spectrochim Acta A* 55:2919–2925
- Guo Y, Zeng XQ, Yuan HY et al (2017) Chiral recognition of phenylglycinol enantiomers based on N-acetyl-L-cysteine capped CdTe quantum dots in the presence of  $\text{Ag}^+$ . *Spectrochim Acta Part A* 183:23–29
- Han D, Yan L, Chen W et al (2011a) Preparation of chitosan/graphene oxide composite film with enhanced mechanical strength in the wet state. *Carbohydr Polym* 83:653–658
- Han DL, Yan LF, Chen WF et al (2011b) Cellulose/graphite oxide composite films with improved mechanical properties over a wide range of temperature. *Carbohydr Polym* 83:966–972
- Jaiseal JK, Mattoussi H et al (2003) Long-term multiple color imaging of live cells using quantum dot bioconjugates. *Nat Biotechnol* 21:47–51
- Jasim A, Ullah MW, Shi ZJ et al (2017) Fabrication of bacterial cellulose/polyaniline/single-walled carbon nanotubes membrane for potential application as biosensor. *Carbohydr Polym* 163:62–69

- Jia MF, Zhang Z, Li JH et al (2017) A molecular imprinting fluorescence sensor based on quantum dots and a mesoporous structure for selective and sensitive detection of 2,4-dichlorophenoxyacetic acid. *Sens Actuators B* 252:934–943
- Junaid M, Imran M, Ikram M et al (2019) The study of Fe-doped CdS nanoparticle-assisted photocatalytic degradation of organic dye in wastewater. *Appl Nanosci* 9:1593–1602
- Li Y, Dong LJ, Wang WP et al (2006) Flow injection analysis–Rayleigh light scattering detection for online determination of protein in human serum sample. *Anal Biochem* 354:64–69
- Li ZS, Xu W, Wang YT et al (2015) Quantum dots loaded nanogels for low cytotoxicity, pH-sensitive fluorescence, cell imaging and drug delivery. *Carbohydr Polym* 121:477–485
- Li GH, Sun KY, Li DW et al (2016) Biosensor based on bacterial cellulose–Au nanoparticles electrode modified with laccase for hydroquinone detection. *Colloids Surf A* 509:408–414
- Liu SP, Yang Z, Liu ZF et al (2006) Resonance Rayleigh-scattering method for the determination of proteins with gold nanoparticle probe. *Anal Biochem* 353:108–116
- Liu LZ, Feng F, Pauw MC et al (2015a) Sensitive determination of kaempferol using carbon dots as a fluorescence probe. *Talanta* 144:390–397
- Liu X, Fu CH, Ren XL et al (2015b) Fluorescence switching method for cascade detection of salicylaldehyde and zinc(II) ion using protein protected gold nanoclusters. *Biosens Bioelectron* 74:322–328
- Liu HY, Dong YS, Zhang BB et al (2016a) An efficient quinoline-based fluorescence sensor for zinc(II) and its application in live-cell imaging. *Sens Actuators B* 234:616–624
- Liu ZZ, Gong Y, Fan ZF (2016b) Cysteine detection using a high-fluorescence sensor based on a nitrogen-doped graphene quantum dot–mercury(II) system. *J Lumin* 175:129–134
- Liu RJ, Zhao JJ, Huang ZR et al (2017a) Nitrogen and phosphorus co-doped graphene quantum dots as a nano-sensor for highly sensitive and selective imaging detection of nitrite in live cell. *Sens Actuators B* 240:604–612
- Liu ZM, Zhang X, Cui L et al (2017b) Development of a highly sensitive electrochemiluminescence sophoridine sensor using Ru(bpy)<sub>3</sub><sup>2+</sup> integrated carbon quantum dots–polyvinyl alcohol composite film. *Sens Actuators B* 248:402–410
- Lu ZS, Chen XJ, Hu WH (2017) A fluorescence aptasensor based on semiconductor quantum dots and MoS<sub>2</sub> nanosheets for ochratoxin A detection. *Sens Actuators B* 246:61–67
- Mansur AAP, de Carvalho FG, Mansur RL et al (2017) Carboxymethylcellulose/ZnCdS fluorescent quantum dot nanoconjugates for cancer cell bioimaging. *Int J Biol Macromol* 96:675–686
- Mao J, Yao JN, Wang LN (2008) Easily prepared high-quantum-yield CdS quantum dots in water using hyperbranched polyethylenimine as modifier. *J Colloid Interface Sci* 319(1):353–356
- Mehrzad-Samarin M, Faridbod F, Dezfuli AS et al (2017) A novel metronidazole fluorescent nanosensor based on graphene quantum dots embedded silica molecularly imprinted polymer. *Biosens Bioelectron* 92:618–623
- Ngamdee K, Kulchat S, Tuntulani T et al (2017) Fluorescence sensor based on d-penicillamine capped cadmium sulfide quantum dots for the detection of cysteamine. *J Lumin* 187:260–268
- Ni Y, Zhang F, Kokot S (2013) Graphene oxide as a nanocarrier for loading and delivery of medicinal drugs and as a biosensor for detection of serum albumin. *Anal Chim Acta* 769:40–48
- Nicholson JP, Wolmarans MR (2000) The role of albumin in critical illness. *Br J Anaesth* 85:599–610
- Nie H, Liu M, Zhan F et al (2004) Factors on the preparation of carboxymethylcellulose hydrogel and its degradation behavior in soil. *Carbohydr Polym* 58:185–189
- Phukn P, Radhapyari C, Konwar BK et al (2014) Natural polyhydroxyalkanoate–gold nanocomposite based biosensor for detection of antimalarial drug artemisinin. *Mater Sci Eng C* 37:314–320
- Ratnesh RK, Mehata MS (2017) Investigation of biocompatible and protein sensitive highly luminescent quantum dots/nanocrystals of CdSe, CdSe/ZnS and CdSe/CdS. *Acta Part A* 179:201–210
- Refat MS, Al-Maydama HMA, Al-Azab FM et al (2014) Synthesis, thermal and spectroscopic behaviors of metal–drug complexes: La(III), Ce(III), Sm(III) and Y(III) amoxicillin trihydrate antibiotic drug complexes. *Spectrochim Acta Part A* 128:427–446
- Robelek R, Niu LF, Schmid EL et al (2004) Multiplexed hybridization detection of quantum dot-conjugated DNA sequences using surface plasmon enhanced fluorescence microscopy and spectrometry. *Anal Chem* 76:6160–6165
- Sasmal M, Maiti TK, Bhattacharyya TK (2015) Synthesis of ZnO nanosphere for picomolar level detection of bovine serum albumin. *IEEE Trans Nanobiosci* 14(1):129–137
- Selvaprakash K, Chen YC (2014) Using protein-encapsulated gold nanoclusters as photoluminescent sensing probes for biomolecules. *Biosens Bioelectron* 61:88–94
- Tang AM, Liu Y, Wang QW et al (2016) A new photoelectric ink based on nanocellulose/CdS quantum dots for screen-printing. *Carbohydr Polym* 148:29–35
- Wang DY, Rogach AL, Caruso F (2002) Semiconductor quantum dot-labeled microsphere bioconjugates prepared by stepwise self-assembly. *Nano Lett* 2:857–861
- Wang L, Wang J, Chen Y et al (2011) One-step synthesis and quantum yield of CdS quantum dots. *Chem J Chin U* 32:1043–1048
- Wang K, Dong YH, Li BY et al (2017) Differentiation of proteins and cancer cells using metal oxide and metal nanoparticles-quantum dots sensor array. *Sens Actuators B* 250:69–75
- Weng H, Yan B (2016) A flexible Tb(III) functionalized cadmium metal organic framework as fluorescent probe for highly selectively sensing ions and organic small molecules. *Sens Actuators B* 228:702–708
- Yadav M, Rhee KY, Jung IH (2013) Eco-friendly synthesis, characterization and properties of a sodium carboxymethyl cellulose/graphene oxide nanocomposite film. *Cellulose* 20:687–698
- Yan YJ, He XW, Li WY et al (2017) Nitrogen-doped graphene quantum dots-labeled epitope imprinted polymer with

- double templates via the metal chelation for specific recognition of cytochrome c. *Biosens Bioelectron* 91:253–261
- Yang CL, Deng WP, Liu HY et al (2015) Turn-on fluorescence sensor for glutathione in aqueous solutions using carbon dots–MnO<sub>2</sub> nanocomposites. *Sens Actuators* 216:286–292
- Yang HY, Fu Y, Jang MS et al (2017) CdSe@ZnS/ZnS quantum dots loaded in polymeric micelles as a pH-triggerable targeting fluorescence imaging probe for detecting cerebral ischemic area. *Colloids Surf B* 155:497–506
- Yu WW, Chang E, Drezek R et al (2006) Water-soluble quantum dots for biomedical applications. *Biochem Biophys Res Commun* 348:781–786
- Yu XF, Chen LD, Li KY et al (2007) Immunofluorescence detection with quantum dot bioconjugates for hepatoma in vivo. *J Biomed Opt* 12:014008
- Zhang HC, Shang YY, Zhang T et al (2017a) Engineering graphene/quantum dot interfaces for high performance electrochemical nanocomposites in detecting puerarin. *Sens Actuators B* 242:492–501
- Zhang N, Zhang L, Ruan Y et al (2017b) Quantum-dots-based photoelectrochemical bioanalysis highlighted with recent examples. *Biosens Bioelectron* 94:207–218
- Zhu W, Xuan C, Liu G et al (2015a) A label-free fluorescent biosensor for determination of bovine serum albumin and calf thy mus DNA based on gold nanorods coated with acridine orange-loaded mesoporous silica. *Sens Actuators B* 220:302–308
- Zhu J, Liu XQ, Wang XH et al (2015b) Preparation of polyaniline–TiO<sub>2</sub> nanotube composite for the development of electrochemical biosensors. *Sens Actuators B* 221:450–457
- Publisher's Note** Springer Nature remains neutral with regard to jurisdictional claims in published maps and institutional affiliations.